atmosphere

MDPI

Article

Formation and Precipitation Processes of the Southwest Vortex Impacted by the Plateau Vortex

Aijuan Bai [1,*], Jinfeng Bai [1,*], Zhao Wang [2] and Chaoyong Tu [1]

[1] College of Atmosphere Science, Chengdu University of Information Technology, Chengdu 610225, China; tuchaoyong@cuit.edu.cn
[2] Shaanxi Meteorological Service Center of Agricultural Remote Sensing and Economic Crops, Xi'an 710015, China; sandstom@163.com
* Correspondence: baiaj@cuit.edu.cn (A.B.); 17519404236@163.com (J.B.)

Abstract: This study investigated the source, trajectory, and precipitation of the Southwest (SW) vortex, which was linked with the Plateau (P) vortex. Based on the statistical study of a number of cases, this study showed the following results. The SW vortex tended to originate at the northeastern and western peripheries of the Sichuan Basin, normally coinciding with the presence of the P vortices in the eastern region of the Tibetan Plateau. Most of the aforementioned vortices exhibited a longer life span, and resulted in severe storms averaging approximately 50 mm of rainfall per day, especially in the cases of more than 100 mm of rainfall per day in eastern and southern China. Furthermore, new findings were obtained: (1) The SW vortex and the P vortex were attributed from an 'Ω' circulation pattern from blocking high in middle to high latitudes region. The SW vortex was notably influenced by the convergence of two air currents. In the lower troposphere, the southwesterly jet of the South Asian monsoon flowed over and around the Yungui Plateau, and cold–dry air from the north flowed into the Basin. (2) Both the SW vortex and the P vortex displayed a shallow synoptic system characterized below 500 hPa, and wet–cold cores formed around the sources at low altitudes. (3) The analysis on atmospheric instability and dynamics suggested that the vortices' eddies generated significant convective instability at lower levels. The circulation pattern and instability conditions facilitated the heavy precipitation associated with the SW vortex, and the ample water vapor and subsequent latent heat intensified the precipitation.

Keywords: Southwest vortex; plateau vortex; heavy rainfall; formation; the Sichuan Basin

check for updates

Academic Editor: Yoshihiro Tomikawa

Received: 28 November 2024
Revised: 7 January 2025
Accepted: 15 January 2025
Published: 22 January 2025

Citation: Bai, A.; Bai, J.; Wang, Z.; Tu, C. Formation and Precipitation Processes of the Southwest Vortex Impacted by the Plateau Vortex. *Atmosphere* **2025**, *16*, 115. https://doi.org/10.3390/atmos16020115

Copyright: © 2025 by the authors. Licensee MDPI, Basel, Switzerland. This article is an open access article distributed under the terms and conditions of the Creative Commons Attribution (CC BY) license (https://creativecommons.org/licenses/by/4.0/).

1. Introduction

The Southwest vortex (referred to as the SW vortex) is a typical subsynoptic scale eddy over the Sichuan Basin (referred to as the Basin). It serves as an important system contributing to precipitation patterns over Southwest China. To be specific, the eddies associated with the SW vortex, especially those with prolonged duration, can cause the majority of the extreme rainfall events and subsequent flooding in Southwest China during the spring and summer seasons [1–8]. Some studies were carried on the Plateau vortex and its formation (referred to as the P vortex) [9–17]. To identify the SW vortex and P vortex, the 700 hPa and 500 hPa levels were selected as the representative altitudes, respectively [18]. The China Meteorology Administration stipulated that there should be a wind eddy observed among three sounding sites situated in distinct quadrants of Southwest China. It was discovered that the SW vortex's eddies typically manifested at specific altitudes within or close to their sources, and their mesoscale characteristics often

made them challenging to be identified. Consequently, an inadequate understanding the structure of the SW vortex and P vortex restricted the prediction of heavy precipitation. Therefore, particular emphasis should be placed on the examination of the vortices.

Lu [2] indicated that the SW vortex commonly appeared within a defined spatial area ranging from 25°–35° N to 100°–110° E. Occasionally, the SW vortex manifested concurrently with, or was subsequent to, the P vortex. Therefore, meteorologists deduced that SW vortices were either triggered or influenced by P vortices [19,20]. For the heavy rainfall from the SW vortex and P vortex, Kuo et al. [21], Ma et al. [22], Xiao and Chen [23], and Wang and Wang [24] detailed that flooding within the Basin primarily originated directly from a prolonged mesoscale eddy of the SW vortex, particularly when such vortices amalgamated with another mesoscale eddy above the northeastern plateau, known as the P vortex. In addition, Liu et al. [25] and Zhang and Duan [26] discovered that strong convective weather frequently increased in the western quadrant of the SW vortex, occasionally extended to the southeastern quadrant. The precipitation associated with the SW vortex primarily comprised short-term heavy precipitation, characterized by intensities ranging from 22 to 32 mm per hour. Due to the coupling and interactions between SW vortex and P vortex, the strong advection of the temperature and humidity was formed in the troposphere over the southeast quadrant of the SW vortex, leading to convective instability and heavy rainfall [22].

Furthermore, existing investigations concerning the SW vortex had primarily addressed its circulation, the formation mechanism, and associated precipitation. In terms of the circulation, Kuo et al. [3] and Zhou et al. [27] highlighted that the SW vortex originated from the southwesterly monsoon flow's nonlinear obstruction of the Yungui Plateau, generating cyclonic relative vorticity at lower altitudes above the Basin through the expansion of the Earth's background vorticity. Also, the flow of the eastern jet was blocked by the elevated terrain of the Tibetan Plateau, which played a significant role in the formation of the vortices [28]. However, other studies highlighted that a SW vortex emerged subsequently to the traversal of westerly winds over the Tibetan Plateau, and the descending of westerly winds into the lower Basin was conducive to the formation of the vortex [29–33]. In addition, Zhao and Wang [34] addressed the interactions between the robust dry–cold easterly jet and the northward warm–humid jet within the Basin, which contributed to the formation of the vortex. Other studies indicated that the terrain and its heat source played a significant role in the genesis of the vortex [13,35].

In terms of the structures of SW and P vorties, several studies highlighted the presence of a warm core, a moist center, vertical upward motion, cyclonic vorticity, and other characteristics within or around the vortex [34,36–40]. For example, Zhao and Wang [34] showed that the SW vortex exhibited a warm core in the 300 hPa temperature field, while in the lower troposphere below 850 hPa, it was warm in the southern and cold in the northern. Additionally, some findings noted the presence of two upward motions on both the northern and southern sides of the vortex, along with a converging motion near its center. Wang and Isidoro [30] identified that the terrain blockage caused by the Tibetan Plateau facilitated the establishment of a conditionally unstable atmospheric setting, which was conducive to the genesis of the SW vortex. In addition, some studies have been conducted to investigate and simulate the vertical structure and precipitation associated with the SW vortex [3,20]. Xiao et al. [20] analyzed the SW vortex accompanied by the P vortex, and they revealed that the mesoscale environment served as the mechanism underlying the SW vortex and its associated precipitation.

From above analysis on vortices, it can be found that many studies had primarily concentrated on either the P vortex or SW vortex separately [9,26], with only a few exploring the characteristics of the SW vortex, which was influenced by the P vortex [19,20]. It is

quite clear that the SW vortex tended to produce heavier precipitation as it was under the influence of the P vortex. Hence, it was imperative to conduct a study on these vortices, especially on the heavy precipitation. Of course, in order to determine the causes of precipitation, the circulation of air flows and the vertical structures associated with the vortices should be explored.

Therefore, in this paper, we focused on the SW vortex associated with the P vortex, laying a particular stress on its circulation, precipitation, and structure. We tried to perform a statistical examination on the characteristics of the SW vortex in correlation with the P vortex. In addition, this study explored both the horizontal and vertical structures of the vortices, along with their associated precipitation. Based on above work, we aimed to answer the following questions: What are the characteristics of the SW vortex associated with the P vortex? What are the formation mechanisms underlying the initiation of precipitation from the interactions between the SW vortex and the P vortex? Indeed, the main aims of this study were to illuminate the characteristics of the SW vortex, as influenced by the P vortex, and to enhance the understanding of the heavy precipitation in Southwest China.

2. Data and Method

2.1. Case Overview

Firstly, the SW vortex cases in this study were obtained from the annual books of the SW vortex, and the cases in the summer months (May to September) from 1998 to 2021 were selected for the statistical analysis and case study. For each case of SW vortex affected by the P vortex, the following conditions must be satisfied. Firstly, it should be confirmed that the circulation of a SW vortex had formed. Then the weather map of 500 hPa from ERA-5 data was checked to determine a P vortex developed too. Furthermore, the P vortex must manifest within a two-day interval either preceding or following the occurrence of the SW vortex [19]. In total, 26 cases spanning the previous 24 years were selected for this investigation into the characteristics of the vortices. From all the cases, 10 representative cases were selected, according to their different sources, routes, and precipitation. Their source location, lifespan, trajectory, and corresponding precipitation are detailed at length in Table A1.

2.2. Dataset

To delineate the precipitation associated with the SW vortex and the P vortex, the data for the sites provided by the China Meteorological Administration were analyzed. During the specified period of time, there were more than 3000 automatic weather stations in Southwest China as well as in the middle and lower reaches of Yangtze River. Because of the sparse sounding observations in the troposphere, the sounding data were insufficient for a thorough investigation into the detailed structures of the vortices. Therefore, this study used the ERA-5 dataset (the fifth generation of the ECMWF global atmospheric reanalysis) obtained from website (https://cds.climate.copernicus.eu/, accessed on 10 January 2024) to examine the synoptic scale and mesoscale characteristics of circulation, temperature, and humidity. The ERA-5 dataset was acquired with a higher resolution of 0.25° for both longitude and latitude. It consisted of 37 vertical levels and was recorded at six-hour intervals. Key components outlined in this study encompassed elements such as geopotential height, horizontal wind, specific humidity, temperature, and so forth. Beijing time is used through this paper.

2.3. Method

We determined the sources of the vortices via the low pressure indicated by the geopotential height from the ERA-5 [18]. Furthermore, to explore the common features

of the SW vortices that were associated with the P vortices, a statistical approach was employed to analyze the characteristics of the source and trajectory of the vortex, along with the specific precipitation. Moreover, the compositing analysis method [41,42] was utilized in this research to examine the common horizontal and vertical structures as well as the precipitation mechanism of the SW vortex. For the compositing analysis, a simulated SW vortex was set up, which was named composite SW vortex and located in the averaged source of all the cases. Then, each SW vortex cases was moved to the composite one, including the centers and associated circulation data. As a result, this composite vortex was centered with the averaged cores and had the common features of the SW vortex associated with the P vortex.

3. Results

3.1. Statistical Analysis of the SW Vortices Associated with the P Vortices

3.1.1. The Source

The source was the fundamental characteristics of the SW vortices and the P vortices. We obtained the source position of every case from the geopotential height in ERA-5 data, and the source was the center of low pressure at the 700 hPa level. From all 26 cases, the source locations of the SW vortices and P vortices were highly concentrated (as shown in Figure 1). In terms of the positions of the P vortices, 20 cases originated within the region of 29.8–35.2° N, 92.1–99.2° E, whereas the remaining 6 P vortices were scattered across the eastern and northeastern regions of the Tibetan Plateau, being outside of the aforementioned area. It was indicated that the majority of the P vortices, which were associated with the SW vortices, tended to form in the eastern region of the Tibetan Plateau.

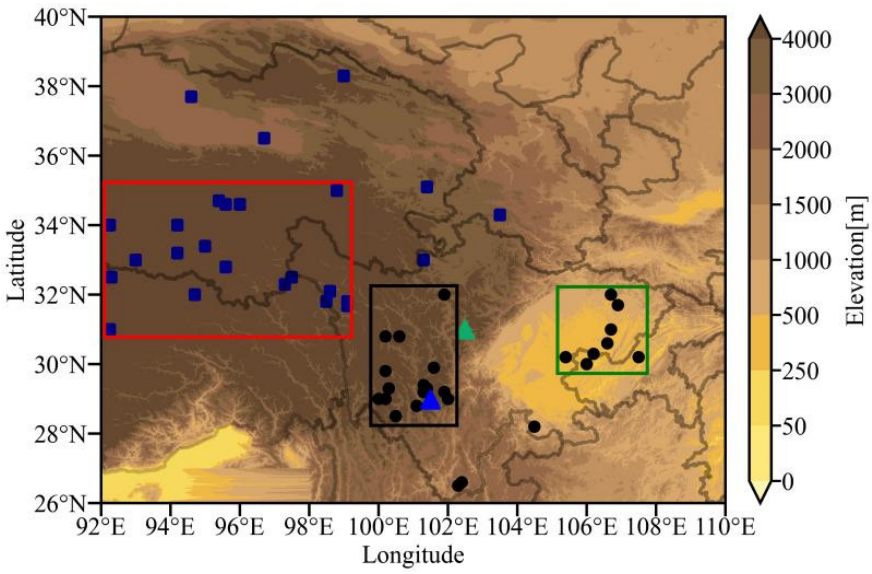


Figure 1. The sources of the P vortices (depicted by blue rectangles) and the SW vortices (represented by the black circles) across the 26 cases. (The shaded areas were the terrain elevation; unit: m. The dashed and solid rectangles denoted the most common locations of the P vortices and the SW vortices, respectively. The blue and green triangles indicated the locations of Jiulong and Xiaojin, respectively).

In terms of the SW vortices, two concentrated regions were observed at the northeastern and western edges of the Basin. Specifically, 15 vortices were situated within the geographical coordinates of 28.3–32.2° N and 99.8–102.2° E, representing the western Sichuan Plateau. The sources of these vortices were concentrated around Jiulong, with fewer vortices dispersed around the Xiaojin area. Additionally, eight cases were situated in

the region of 29.8–32.2° N and 105.2–107.7° E, at the northeastern edge of the Basin. Finally, there were 3 SW vortex cases that could not be included in the two aforementioned regions.

The P vortex was a distinctive synoptic system observed over the Tibetan Plateau. Chen et al. [15] noted that this vortex primarily developed within the region ranging from 30° N to 35° N, west of 95° E, commonly referred to as the area north of Naqu or located between Kunza and Gaize. Feng et al. [17] identified that the most concentrated source of the P vortex was situated in the high-altitude regions of the central and western Tibetan Plateau, spanning from 33° N–36° N to 84° E–90° E. The findings of this research agreed with Chen et al. [15] in the sources of the P vortices, albeit positioned to the east relative to the findings of Feng [17]. Overall, the P vortex associated with the SW vortex was different from other P vortices in the sources.

Regarding the origins of the SW vortex, prior research affirmed the presence of three sources: Jiulong, Xaiojin, and the Sichuan Basin [32]. He [8] highlighted that the SW vortex predominantly manifested in the western Sichuan Plateau, specifically in the regions such as Jiulong, Batang, and Kangding, but occasionally the SW vortex was stationary within the Basin. Huang [41] investigated the composite positions of 16 SW vortices and determined that they were positioned approximately 30.6° N and 103° E, situated northeast of Jiulong and spanning a distance of approximately 200 km. The investigation conducted by Huang [41] focused mainly on the stationary SW vortices. Our study centered on the SW vortex associated with the P vortex, and observed a tendency for these SW vortices to manifest within the two selected fixed areas. In detail, the western source in our study aligned with those of Huang [41] and He [8], identifying these eddies as the Jiulong and Xiaojin vortices. The eastern source was correlated with the Basin vortex, predominantly dispersing in the northeast of the Basin.

3.1.2. The Time Disparity

This study explored the time disparity between the formation of the SW vortices and the P vortices, based on the all cases, especially on the cases outlined in Table A1. Among the 10 representative cases of SW vortices associated with the P vortices, there was just one case in which the SW vortex emerged prior to the P vortex. Moreover, in 24 out of 26 cases, the SW vortices were detected subsequently to the occurrence of the P vortex. In addition, among the 24 cases, 18 exhibited a formation of the SW vortices occurring more than 24 h after the P vortex, while in the remaining 6 cases, the SW vortices were observed approximately 12 h after the P vortices. In summary, a prevailing pattern was revealed in which the SW vortices tended to appear after the P vortices, indicating that the SW vortex was almost triggered by the P vortex. The time difference between the occurrence of the SW vortex and that of the P vortex observed in this study agreed closely with the results reported by Zhao and Wang [34], but more importantly, we pointed out the most likely specific time of more than 24 h. Thus, if P vortices were detected in the northeastern region of the Tibetan Plateau, within a day or possibly half a day, SW vortices might potentially develop over the western Sichuan Plateau or the central and northeastern areas of the Basin.

3.1.3. The Trajectories

The analysis involved the examination of ERA-5 data collected at six-hour intervals to assess the trajectories of the vortices cases. Based on the cases in Table A1, 8 SW vortices exhibited a similar trajectory, wherein they typically propagated eastward, traversing the middle and lower reaches of the Yangtze River, and ultimately disappeared into the East Sea. Additionally, there were two SW vortices that remained stationary within the Basin. More studies based on all 26 cases discovered that the majority of the SW vortices influenced by the P vortex displayed a predominant eastward movement, impacting the

region of East China. These vortices typically culminated their trajectory in the East China Sea or the Pacific Ocean.

Taking the case of 5 August 2019 in Table A1 as an example, the P vortex initially manifested at 08:00 on 5 August over the northeast of the Tibetan Plateau at an altitude of 600 hPa. Following that, the SW vortex appeared at 08:00 on 6 August at 850 hPa on the southern boundary of the Basin. This SW vortex experienced an approximately one-day delay relative to the P vortex. Meanwhile, as the P vortex advanced eastward, it divided into two segments. Furthermore, one eddy moved towards the northeast direction and was identified as the northwest China vortex. On the contrary, the second eddy moved towards the southeast direction and followed a trajectory similar to the SW vortex. In addition, the SW vortex remained situated over the western Sichuan Plateau during the initial day before proceeding along an eastward route. Finally, the SW vortex moved out of China and dissipated into the East China Sea at 02:00 on 8 August. In conclusion, the SW eddies exhibited a lifespan of approximately 3 days, characterized by a prolonged duration. For this process of the SW vortex, there was heavy precipitation not only in the central of Basin, but also in the East China Sea, with extreme daily precipitation of 109 mm. The above example analysis showed that the SW vortex was triggered by the P vortex, and they resulted in heavy precipitation.

In each of all the cases, the trajectories of the P vortices closely resemble those outlined by Guo [9], who noted that the majority of the P vortices tended to exhibit a northeasterly orientation. Additionally, nearly all the SW vortices in this study followed a typical eastward trajectory. Based on the findings of the case study, it can be concluded that the SW vortex with the P vortex exhibited an extended lifespan and a directional movement towards the East China Sea along an easterly path. The long lifespan and eastward trajectory were the main characteristics of this type of SW vortex and P vortex.

From above analysis of the trajectories of the SW vortices, it can be concluded that the SW vortices triggered by the P vortex generally propagated eastward, and sometimes they stayed around the Basin. Nevertheless, following their passage through the extensive middle and lower sections of the Yangtze River, the SW vortices generally tended to disappear in the East China Sea. As a distinct subset of the SW vortices, they demonstrated greater strength and prolonged duration compared to other SW eddies observed previously. As a result, this study indicated that both P vortices and SW vortices can endure for extended periods and disperse extensively in the lee side of the Plateau. However, some previous research noted that the SW vortices used to remain stationary or circulated around the Basin [41].

3.1.4. Precipitation

It had been demonstrated that the SW vortices usually generated significant precipitation around their cores when they remained in the Basin or moved towards the east [27,31]. Therefore, the precipitation of SW vortices extended significantly across the expansive area of the Basin, as well as across the southwest and the eastern regions of China. In essence, the prevalence of numerous severe flood disasters in and around the Yangtze River have been linked to the influence of the SW vortices.

The examination of the representative cases listed in Table A1 showed the following conclusions. First, the cyclone's formation in the vicinity of the Basin resulted in substantial precipitation in the local districts. There were nine vortices that caused heavy rainfall exceeding 50 mm within a 24 h timeframe. Occasionally, the SW vortex was accompanied by moderate precipitation. For instance, in the scenario of 13 May 2013, the 24 h rainfall amounted to approximately 30 mm. Secondly, when a mature SW vortex exited the Basin, it tended to induce substantial precipitation in the middle and lower reaches of the Yangtze

River, often exceeding 90 mm per day in most cases. Extreme precipitations of downpour occurred in two cases of 29 June 2013 and 8 July 2016, respectively reaching maximum daily amounts of 273 mm and 210 mm, as the vortices departed the Basin.

The precipitation associated with SW vortex was examined in detail by the case of 5 August 2019 (as shown in Figure 2). At 20:00 on 5 August, a SW vortex formed in the southern region of Sichuan Province. Until 00:00 on 6 August, a low pressure of 310 dagpm was exhibited (Figure 2a). Simultaneously, the ground observation recorded precipitation commencing on the northwest side of the low, with the daily precipitation exceeding 50 mm. By 00:00 on 7 August, the SW vortex reached its maturity state, and subsequently moved toward to Chongqing (as shown in Figure 2b). Then the low pressure intensified to 309 dagpm, resulting in a significant expansion of the precipitation area. At that time, the main storm center was situated in the west side of the SW vortex, positioned southwest of the Basin. The precipitation of this SW vortex covered the extensive regions of eastern Chongqing, southern Shaanxi and Hubei. Following the departure of the SW vortex from the Basin and its presence in the eastern plains of China, extreme heavy precipitation of 109 mm was recorded within a 24 h period.

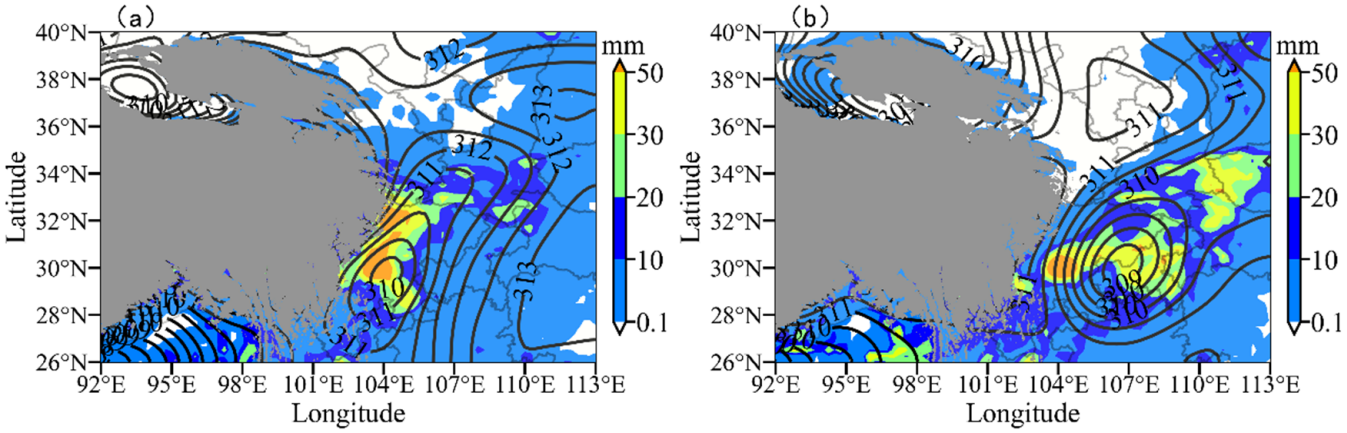


Figure 2. The horizontal distribution of geopotential height at 700 hPa (contour; unit: dagpm) and 24 h precipitation amount (shadow; unit: mm) at 00:00 on 6 August (**a**) and at 00:00 on 7 August 2019 (**b**). The gray shadow covered the areas with an altitude of more than 1500 m.

In fact, the case of 5 August 2019 yielded notable precipitation, impacting not only the Basin, but also the eastern and southern regions of China. Although there was increased precipitation in the northwestern part of the SW vortex within the Basin, more heavy precipitation occurred in the western and southern part of the eddy within the middle downstream area of the Yangtze River. In general, extreme precipitation exceeding 100 mm per day was the predominant characteristic of the SW vortices, particularly upon their transition to the eastern region of China.

3.2. The Structure of the Vortex

In order to discover the mechanisms and characteristics of the SW vortex induced by the P vortex, the method of composite analysis was conducted on all the cases of SW vortices. Subsequently, the horizontal and vertical structures of the SW vortex and the P vortex were delineated by the composite analysis, elucidating their common characteristics based on the background circulation, water vapor, and temperature fields.

3.2.1. Circulation

The streamlines and the geopotential height of the composite SW vortex are illustrated Figure 3, representing a typical horizontal plane of the vortex. At the 700 hPa height level

depicted in Figure 3a, the primary circulation exhibited a low–high–low pattern in the higher latitudes area of China, alongside a blocking high developed notably northwards. Hence, the meridional air waves experienced intensification, leading to a prominent intersection between the cold and warm air streams. As the eastern low trough strengthened southwards, a cut-off low behind the trough from the north resulted in the formation of SW vortex. The low eddy of the SW vortex was located at the boundary between Sichuan and Chongqing, at the coordinates 29.8° N, 106.8° E. According to the streamlines depicted at the 600 hPa level in Figure 3b, another low trough located in the west of the blocking high influenced the formation of the P vortex in the northeast Plateau and southern Gansu. The P vortex was identified at the coordinates 37.2° N, 95.8° E, exhibiting its most robust cyclonic circulation on the Qinghai Plateau.

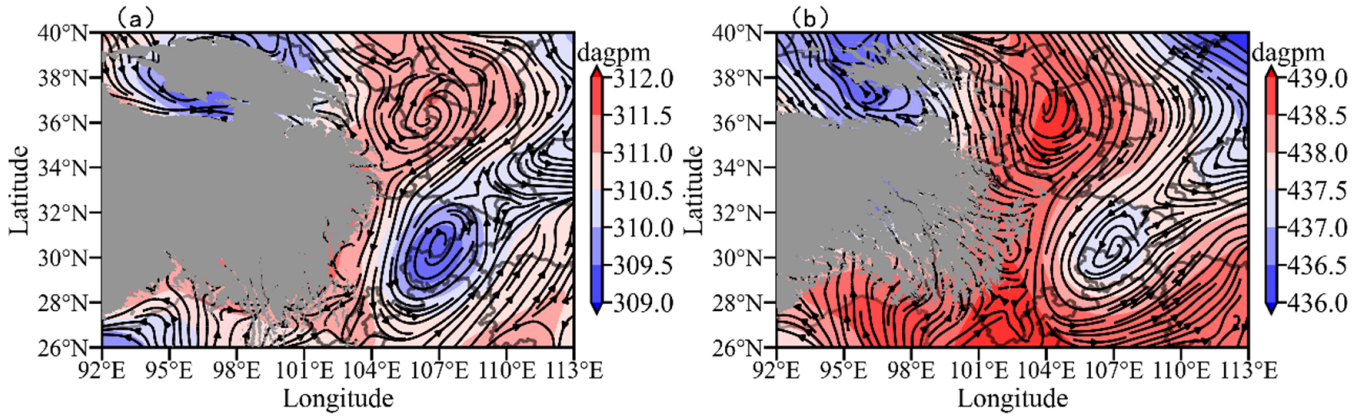


Figure 3. The streamlines (contours) and geopotential height (shadows; unit: dagpm) at 700 hPa (**a**), and 600 hPa (**b**) of the composite SW vortex. (The region covered by the gray shadow had a height of more than 3000 m in (**a**) and 4000 m in (**b**)).

From the above analysis, it was implied that with the development of a blocking high in middle and high latitudes, the meridional wind intensified significantly, corresponding to the pattern of one ridge and two troughs. Two low troughs located in the west and east sides of the blocking high, and progressed towards the east and northeast regions of the Tibetan plateau. In this atmospheric circulation pattern, the southward movement of cold air led to the formation of a SW vortex and P vortex at the base of two low troughs. Consequently, the precipitation developed to the west of the SW vortex.

Furthermore, a profound trough associated with the terrain was delineated, spanning from the northern to the southern region along the eastern boundary of the Plateau in Figure 3. Subsequently to this trough, a vigorous northeasterly wind initiated the conveyance of cold–arid advection directly into the Basin. Simultaneously, the monsoonal southwesterly flowed along the eastern boundary of the Basin, and exhibited a northward displacement, accompanied by the transport of warm air masses. Consequently, a SW vortex emerged as a result of wind shear originating from the north wind and the monsoon, facilitated by the interaction of cold and warm air masses. Meanwhile, the pronounced horizontal wind shear prevailing around the Basin terrain induced a cyclonic whirl in the atmosphere. Huang [41] identified three airflow branches across both the upper and lower troposphere contributing to the formation of a SW vortex, and two of the air flows were similar to this study. The robust airflow originating from South Asia in the upper troposphere of Huang [41] was not be depicted in Figure 3.

It is worth emphasizing that the SW vortex exhibited a strong monsoonal southwestern jet. During summer, the low-level jet experienced a northward displacement following the establishment of the monsoon system over East Asia. Its trajectory transited from a

southern direction over the Yungui Plateau, with its western path subsequently shifting to a southwesterly direction. In conclusion, the warm and humid-laden air masses descended into the Basin. Throughout this process, either the Yungui Plateau or the eastern vicinity of the Tibetan Plateau, along with the Basin, significantly contributed to the genesis of the SW vortex, which was highlighted by Cheng and Guo [28] and Yu [10]. In summary, the distinctive terrain surrounding the Basin greatly induces the cyclonic circulation of the SW vortex.

The structure of both the SW vortex and the P vortex was analyzed by examining the geopotential height profile in the composite case. In Figure 4a, at the 500 hPa level, the interactions between the SW vortex and the P vortex resulted from the robust blocking high exhibiting an 'Ω' pattern over the western part of China. This pattern was accompanied by two low troughs positioned on the blocking high's east and west flanks, and a similar circulation was observed at the 700 hPa level. The SW vortex and the P vortex were situated on the opposite sides of the 'Ω' pattern from the blocking high, coinciding with the westward extension of the easterly low trough across the west of the Basin. The SW vortex originated beneath the low, while the P vortex interacted with the low center. Under this situation, the northwesterly flow intensified, and resulted in the influx of cold air into the Basin.

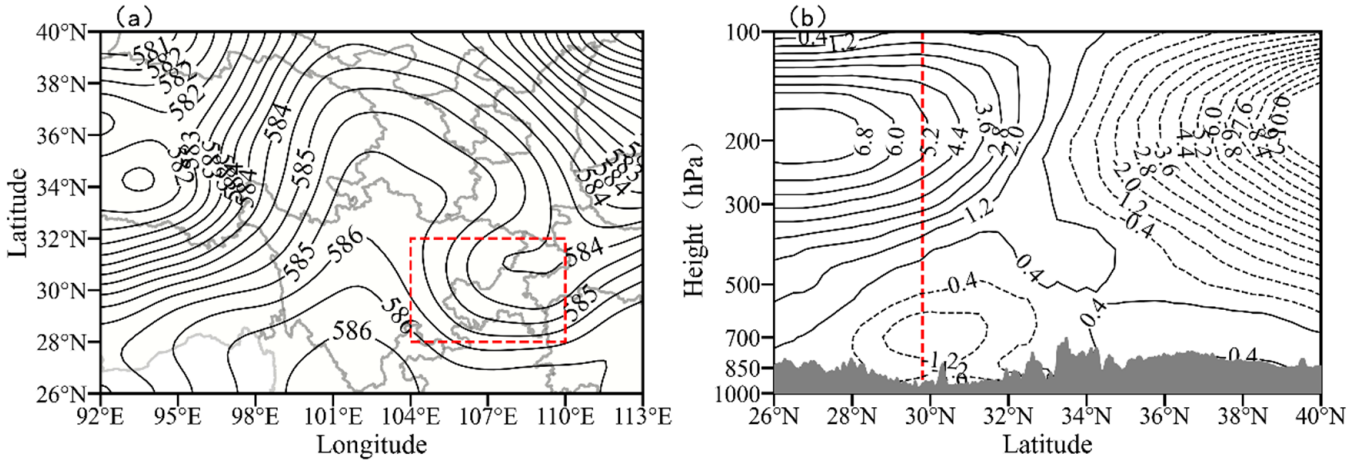


Figure 4. The distribution of geopotential height at 500 hPa (**a**) and its latitude–altitude profile along 106.8° E, the core of the composite SW vortex. (The red dashed line showed the position over the composite SW vortex, and the gray shadow in (**b**) was the terrain).

In the latitude–altitude profile of geopotential height along the center of the composite SW vortex (106.8° E, 29.8° N), as shown in Figure 4b, a pool of low pressure was evident below the 700 hPa level surrounding the vortex, exhibiting a negative anomaly of −1.2 dagpm in geopotential heigh at the 850 hPa level. However, the negative abnormality was substituted with the positive value in the upper layers, indicating a high-pressure system situated above the SW vortex. The positive value originated from the intensification of the South Asian high in the upper troposphere, with the abnormal value exceeding 6.8 dagpm at its center (as shown in Figure 4b). Within the Plateau region situated north of 33°N, the middle troposphere level was influenced by a negative abnormaly initiated by the trough circulation over the north of China. It was verified that the SW vortex observed in the geopotential height field was a shallow system that emerged in the lower troposphere, specifically below 500 hPa.

The above analysis exhibited the vertical structure of the SW vortex that was associated with the impact of the South Asian high in the upper troposphere, and the blocking high and ridge on the eastern side of the Plateau evolved at the middle altitudes. Additionally,

the combination of the P vortex and the SW vortex occurred over the northwest and southeast regions of the ridge. Consequently, the westerly airflow was substituted by the northerly and southerly, leading to the influx of cold air into the Basin, which contributed to the genesis of the SW vortex and the associates vortex precipitation.

3.2.2. Temperature

Several studies have addressed the wet–warm core of the SW vortex within the troposphere, and emphasized that it is a prominent characteristic of the vortex [3,39]. Regarding the thermal characteristics of vortices, Figure 5a illustrates the temperature field distribution at the 700 hPa level from the composite case. Due to the blocking high at the middle to high latitudes, the warm ridge extended northward, and its temperature was 10 °C higher than that of other regions at the same latitude. For the cold northeasterly flow preceding along the blocking high, the temperature at the center of the SW vortex was around 10~12 °C, exhibiting a 2 °C decrease compared to its adjacent areas. Simultaneously, the P vortex exhibited a relative cold core, with the accumulation of cold air masses originating from the northwesterly direction behind the blocking high. It was concluded that the SW vortex and P vortex all exhibited the structure characterized by a cold core.

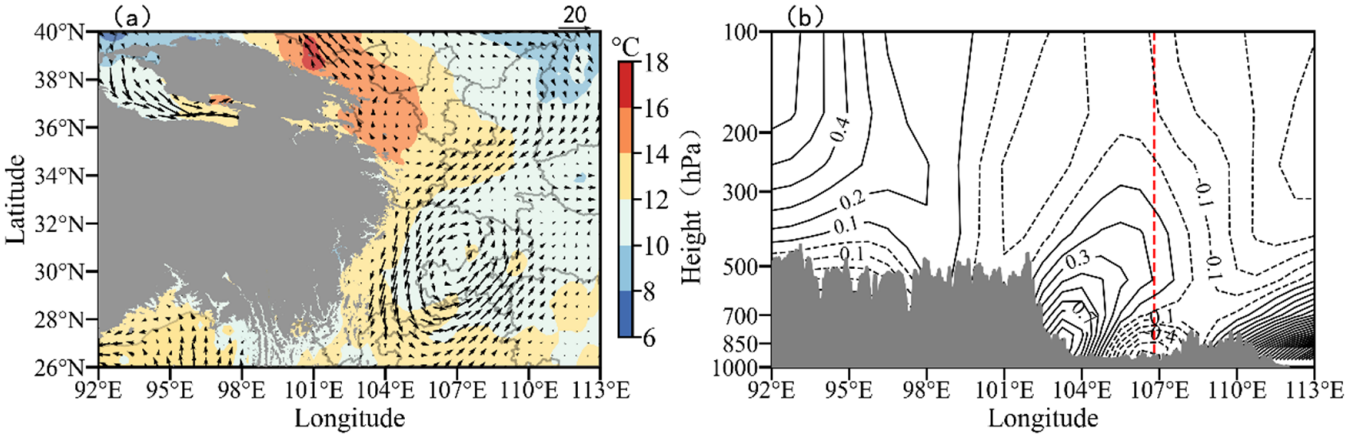


Figure 5. The distribution of the wind (unit: m/s) and temperature fields ((**a**): unit: °C), as well as the longitude–altitude profile of the temperature abnormality ((**b**): solid lines: positive deviation; dashed lines: negative deviation; unit: °C) along the core of the composite SW vortex at 29.8° N (the gray shadow indicated the terrain).

In the temperature profile depicted in Figure 5b, a negative temperature abnormality was highlighted surrounding the SW vortex below the 700 hPa level, with a minimum value of less than −0.4 °C recorded at its center. To the west of the SW vortex, a region with a positive temperature abnormality was identified, corresponding to the warm ridge in Figure 5a. Within the longitudinal range of 92~98° E, the P vortex displayed a shallow negative temperature abnormality at the 500 hPa level. Therefore, the SW vortex and the P vortex showed a core of cold air in the temperature field. The shallow cold cores of the vortices observed at lower altitudes were not consistent with the warm structure identified in prior research documented by Lu [2], Wang and Wang [24], Peng and Cheng [33], Fritsch et al. [36], and Chen and Miao [38]. Regarding the cold core, the SW vortices associated with the P vortices exhibited a distinct structure, which was different from other eddies.

Based on the analysis of both horizontal and vertical profiles in the temperature fields of the vortices, it was evident that the SW vortex and the P vortex exhibited a clearly defined shallow low-pressure core extending from the lower troposphere up to the 500 hPa level. The two vortices interplayed and generated analogous cold air cores within the

low-pressure area of the vortex, which extending towards the eastern part of the Basin at lower altitudes.

3.2.3. Water Vapor

As shown in the composite case in Figure 6, the specific humidity over the center of the SW vortex reached higher values of around 20 k/kg between 800 hPa and 400 hPa, as well as in its southern and northern regions, particularly below the 700 hPa level. Also, there was a pronounced moist core observed near the ground, and as the altitude increased, the specific humidity amount experienced a significant decrease. At the level of 500 hPa, water vapor distribution was constant, with specific humidity value falling below 4 k/kg.

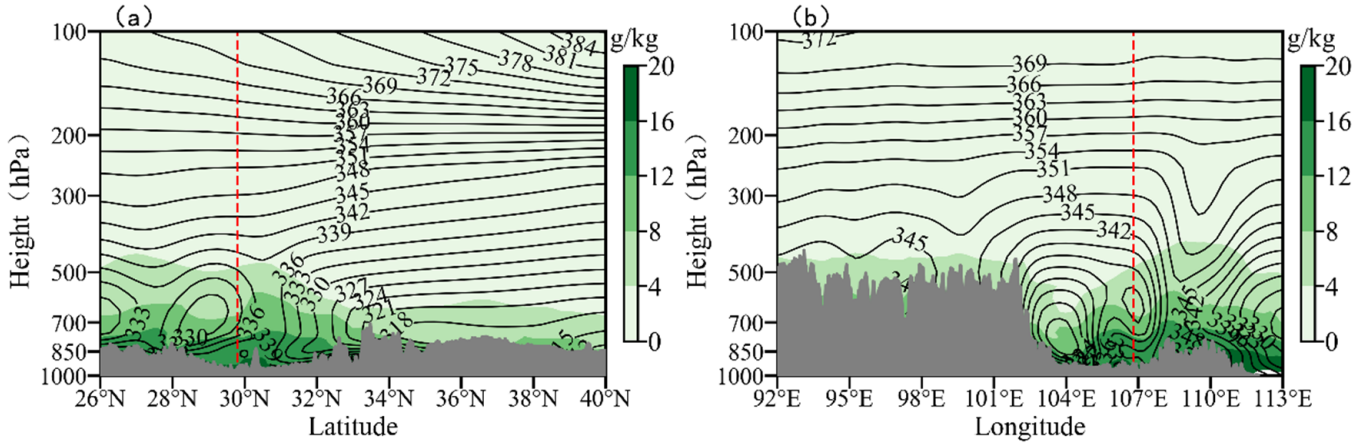


Figure 6. The profile of the false equivalent potential temperature (contour, unit: K) and the specific humidity (shaded, unit: g/kg) of latitude–altitude (**a**) and longitude–altitude (**b**) along the composite SW vortex center (the gray shadow was the terrain of the Tibetan Plateau, and the red dashed lines represented the center of the composite SW vortex).

Meanwhile, a prominent moist tongue was examined evidently at lower altitudes, with a maximum specific humidity value of 16 g/kg, indicating the presence of a moist core extending upward. Beyond that, in the longitude–altitude profile presented in Figure 6b, a lower specific humidity value passage was observed over the western of the SW vortex due to the northerly winds preceding the blocking high. Consistently, at the location of the P convex, a relatively moist area was identified, promoting the intensity of the vortex precipitation.

Consequently, both the SW vortex and the P vortex presented wet cores around their sources. The moist cores, situating at a lower level, played a primary role in releasing latent heat into the troposphere. The wet cores facilitated the formation of the SW vortex and its associated precipitation. However, throughout the evolution of the wet cores, the high latent heat was predominantly released at lower and middle altitudes, indicating that the moist water vapor condensed as a result of upward motion, supplying substantial potential heat to the vortex. Once more water vapor was transported upwards through an ascending motion, greater heat was released through condensation around the vortex. Given the thickness of the vortex, it facilitated deep convection and substantial precipitation within the troposphere.

3.3. Mechanism of the Vortex's Precipitation

In nearly all cases of the SW vortices associated with the P vortices, heavy precipitation was observed, necessitating an exploration of the mechanism behind the vortex precipitation. In the subsequent analysis, meteorological parameters such as false equivalent potential temperature and vorticity were utilized on the composite case, to investigate the

dynamic convective instability and cyclonic motion associated with the precipitation of the SW vortices.

3.3.1. Convective Instability

The false equivalent potential temperature served as a crucial parameter for assessing the stability of the atmosphere. From the latitude–altitude profile over the composite case depicted in Figure 6a, it was evident that the contours of false equivalent potential temperature remained horizontal north of 33° N, with values increasing upward. Indeed, this pattern indicated a stable layered structure in the atmosphere. In the troposphere below the 500 hPa level between the latitude belt of 31° N and 33° N, the contours displayed an upright orientation, indicating a neutral state at lower levels. However, in the south latitude of 31° N, the contours decreased rapidly with a height below the 700 hPa level, showing a pronounced increase in potential instability in the south of the SW vortex. The contours exhibit a similar distribution in Figure 6b, indicating a marked potential instability of the SW vortex.

Hence, the SW vortex induced static instability, and notably, there was sufficient water vapor surrounding the eddy in the Basin. Simultaneously, the upward motion was intensified originating from the Plateau terrain. The release of instability energy from the terrain and potential heat due to the water vapor contributed to the development of strong convection and precipitation. Moreover, water vapor exhibited a positive feedback effect, whereby the instability promoted the upward movement, and led to condensation, heating of the air, and a corresponding increasing upward motion. So the instability and latent heat release from ample water vapor increased and set up a positive feedback cycle, which greatly intensified the precipitation.

3.3.2. Dynamic Analysis

The vorticity of the composite SW vortex was utilized to analyze the mechanism of heavy precipitation surrounding the eddy. Figure 7a depicted the baselines of the profiles in the other three figures of Figure 7. One line is positioned along the connecting line between the SW vortex and the P vortex, while the other lines represent the latitudinal and meridional profiles intersecting the SW vortex. In the vorticity profile along the connection of SW vortex and P vortex depicted in Figure 7b, the strongest positive vorticity of 7 $\times$ 10^{-5}/s can be observed at 107° E, 29.7° N, corresponding to the center of the SW vortex. Additionally, the deep positive vorticity extends from the ground surface to the top of the troposphere.

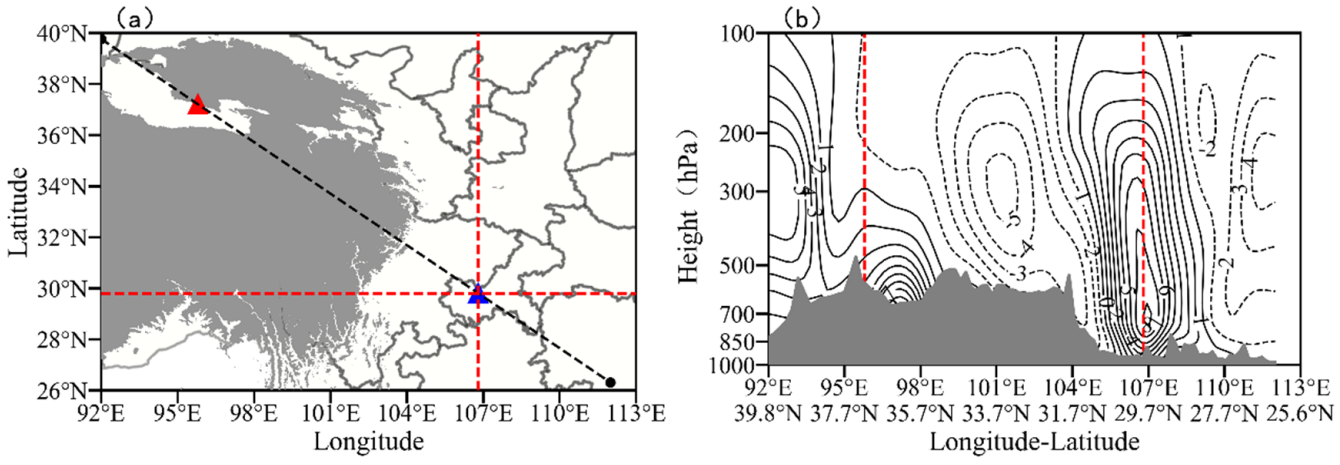


Figure 7. *Cont.*

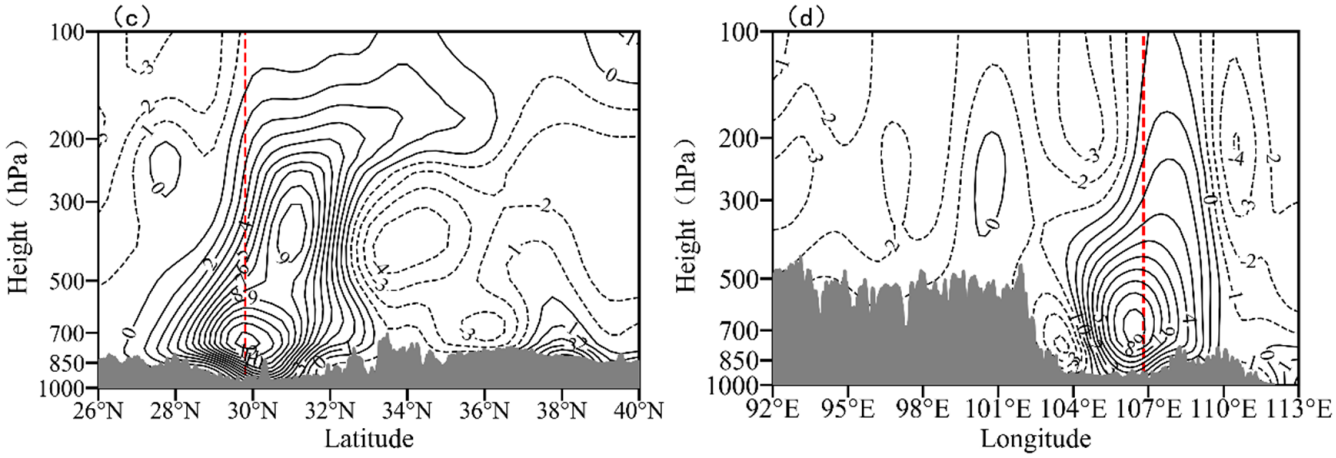


Figure 7. The vorticity profile of the composite SW vortex (unit: $\times 10^{-5}$/s). (**a**): The baseline of (**b**–**d**); (**b**): the vertical distribution along the composite SW vortex, with the red line denoting the position the SW vortex; (**c**): the longitude–elevation distribution along 106.8° E; (**d**): the latitude–elevation distribution along 29.8° N, with the gray shadow representing the terrain of the Tibetan Plateau.

In Figure 7c, the maximum positive vorticity values can be observed at the levels from 700 hPa to 850 hPa, exceeding 9×10^{-5}/s, addressing the presence of a strong cyclonic circulation around the SW vortex with the decreased eddy above and below the SW vortex. Additionally, at the 400 hPa level, a relatively minor but strongest vorticity center was located to the north of the SW vortex. It can be seen that the P vortex overlaied the SW vortex in the troposphere. In the lower latitudes, the presence of an anticyclone originating from the South Asia high was detected in the middle and upper troposphere. Figure 7d illustrates the positive vorticity values of cyclone circulation over the origin of the SW vortex, while negative values due to the anticyclonic circulation to the west and east of the SW vortex can be observed.

The preceding analysis demonstrated that the vorticity of both the SW vortex and the P vortex can extend vertically from the ground to the top of the troposphere, indicating that the SW vortices were dynamic systems with considerable depth. Simultaneously, the low-level cyclone of the SW vortex was associated with the South Asian high at higher altitudes, thereby enhancing the atmospheric baroclinity. Therefore, the high-altitude divergence arising from the convergence of the SW vortex led to the vertical motion and stormy precipitation in the vicinity of the SW vortex.

4. Discussion

Compared with the existing studies about vortex, this paper paid more attention to the special category SW vortex, which was associated with P vortices. We found some distinct characteristics about the vortices, different from other studies. For example, these SW vortices had a longer lifetime, and trended toward propagating eastward, and brought heavy precipitation. There were a lot of SW vortices that disappeared quickly and resulted in light precipitation, as described by Feng [17]. As a highlight of this study, we put forward the unusual circulation of 'Ω' circulation pattern that contributed to the formation of the SW vortex. Furthermore, the two air currents associated with the SW vortex were set up to declare the synoptic systems that resulted in the eddy circulation. More importantly, the precise vertical structure of the SW vortex in temperature and humidity fields was confirmed to explain the formation of the precipitation of the vortices.

In the studies of the SW vortex, precipitation area and intensity were the focus of attention. Kuo et al. [3] and other researchers consolidated findings indicating that the majority of the precipitation related to the SW vortex was concentrated over the northern

region of the eddy circulation, with occasional precipitation occurring within the center of the low-pressure eddy. Zhang and Duan's [26] research discovered that substantial precipitation occurred in the southwestern quadrant of the SW vortex. This study verified that most of the SW vortex cases associated with the P vortex can bring heavy rainfall, and highlighted the extreme rainfall that occurred when they moved eastward, but the precipitation areas relative to the center of SW vortices were not consistent, which meant that the precipitation position was different in each case. If more case studies and more in-depth observations were carried on, the precipitation of the SW vortex associated with the P vortex can be discovered in detail.

5. Summary and Conclusions

This study examined the SW vortex associated with the P vortex, and the findings can be summarized as follows.

Based on a statistical analysis of cases of SW vortices associated with P vortices, this study investigated the sources, trajectories, and precipitation of these vortices. As a specific category of SW vortices, they typically originated from the northeastern and western edges of the Basin, often coinciding with the P vortices located to the northeast of the Tibetan Plateau. These SW vortices and P vortices displayed long lifespans and eastward trajectories. Furthermore, they can resulted in heavy precipitation usually. Once they left the Basin and propagated eastward, they can cause much heavier precipitation in eastern and southern China, impacting the middle and lower reaches of the Yangtze River.

Our detailed examination of a composite SW vortex provided insight into the synoptic circulation background. At the 500 hPa level, the SW vortex and the P vortex were generated by an 'Ω' circulation pattern, influenced by a blocking high-pressure system in the middle-latitude region. Two significant air flows played a substantial role in the SW vortex. First, the southwesterly jet associated with South Asia monsoon at 850 hPa level traversed the Yungui Plateau before descending into the Basin from the eastern side of the vortex. Simultaneously, dry–cold north wind penetrated the Basin at the 600 hPa in front of the blocking high. They converged and created the horizontal wind shear conducive to the cyclonic movement of the SW vortex. Throughout this process, the Yungui Plateau and the Basin exerted considerable influence on the alteration of the wind direction and the establishment of the cyclonic circulation.

In the geopotential height of the composite analysis, both the SW vortex and the P vortex manifested as shallow synoptic circulation systems developing in the lower troposphere below the 500 hPa level. Similarly, the clear cold and moist cores were observed in the SW vortices and P vortices at the low levels. More differently, the vorticity field indicated that the SW vortex and the P vortex can extend vertically from the surface up to the top of the troposphere, representing dynamic deep systems.

Regarding the mechanism of precipitation associated with the SW vortex, the vortex circulation induced significant convective instability at a lower level, while the strong vorticity from the ground to the upper troposphere led to the convergence of water vapor and momentum. The convergent action and instability facilitated heavy precipitation associated with the SW vortex. Moreover, during the course of the SW vortex and P vortex, the ample water vapor, along with its positive feedback effect of latent heat release, enhanced the intensity of the precipitation.

Author Contributions: The project was suggested by Z.W. Analysis performed by A.B. and J.B. Data and comments contributed by A.B. and C.T. All authors revised it critically for important intellectual content. All authors have read and agreed to the published version of the manuscript.

Funding: This work was supported by Natural Science Foundation of China (grant No. U2242202), Natural Science General Project of Shaanxi Provincial (grant No. 2023-JC-YB-279), Key R&D Program for Social Development in Yunnan Provincial (grant Nos. 202203AC100006, 202203AC100005), Research Fund of Chengdu University of Information Technology (grant No. KYTZ376016).

Institutional Review Board Statement: Not applicable.

Informed Consent Statement: Not applicable.

Data Availability Statement: The original contributions presented in the study are included in the article, and further inquiries can be directed to the corresponding author.

Conflicts of Interest: The authors declare that the research was conducted in the absence of any commercial or financial relationships that could be construed as potential conflicts of interest.

Appendix A

Table A1. Introducing the synoptic cases of the SW vortex associated with the P vortex.

No.	P Vortex		SW Vortex		Movement Direction	Precipitation Location and Intensity [2]	Maximum [3]
	Initial Position	Initial Date/Time	Initial Position [1]	Initial Date/Time			Unit: mm
1	35N/96E	2007.7.15/08:00	31.8N/100.5E	7.16/08:00	Eastward	Rainstorm in the northeast part of the Basin.	95
2	34.2N/99E	2012.7.20/08:00	30.8N/102E	7.21/08:00	Eastward	Heavy downpour and rainstorm in the southeast part of the Basin.	188
3	33.4N/95E	2013.5.13/20:00	30.0N/105.0E	5.14/08:00	Eastward	Moderate rain in the northeast of the Basin.	110
4	33.2N/94.2E	2013.5.24/08:00	29.0N/105.0E	5.23/08:00	Eastward	Rainstorm in the northwest of the Basin.	105
5	34N/94.2E	2013.6.4/20:00	30N/107.0E	6.5/08:00	Eastward	Rainstorm in the northeast part of the Basin.	90
6	34.6N/95.6E	2013.6.29/08:00	29.5N/105.0E	6.30/08:00	Stationary	Rainstorm in the northeast part of the Basin.	273
7	32N/106.6E	2014.7.4/08:00	29.0N/104.0E	7.5/08:00	Eastward	Rainstorm in the south part of the Basin.	102
8	34N/92.2E	2016.7.8/08:00	30.8N/100.2E	7.9/08:00	Eastward	Heavy downpour and rainstorm in the western part of the Basin.	210
9 [4]	31.2N/92.2E	2019.8.5/08:00	29.8N/100.2E	8.6/08:00	Eastward	Rainstorm in the central region of the Basin.	109
10	33N/93.2E	2021.9.3/08:00	31.8N/101E	9.4/08:00	Stationary	Rainstorm in the northeast part of the Basin, and in south Shaanxi.	107
Common characteristics	33N/96.7E	6.8/08:00	29.1N/101E 30.8N/106.5E	6.9/08:00	Eastward	Storm in the northeast part of the Basin.	273

Comments: [1] Two predominant positions for the SW vortex were identified, notably at the northeastern and western peripheries of the Basin. [2] The precipitation intensity denoted moderate rain, rainstorms, and heavy downpours from the volume of precipitation recorded during the initial 24 h following to the formation of the SW vortex. [3] The maximum value was recorded during the periods of extreme 24 h precipitation when the SW vortex exited the Basin and moved along the Yangtze River. [4] The ninth case, on 5 August 2019, with shadowing serves as a representative case.

References

1. Tao, S.Y.; Ding, Y.H. Observational evidence of the influence of the Qinghai-Xizang Plateau on the occurrence of heavy rain and severe convective storm in China. *Bull. Am. Meteor. Soc.* **2021**, *62*, 23–30. [CrossRef]
2. Lu, J.H. *Overview of Southwest Vortex*; Meteorological Press: Beijing, China, 1986.

3. Kuo, Y.H.; Cheng, L.S.; Bao, J.W. Numerical simulation of the 1981 Sichuan flood. Part I: Evolution of a mesoscale southwest Vortex. *Mon. Weather. Rev.* **1988**, *116*, 2081–2105. [CrossRef]
4. Zhao, D.J.; Jiang, Y.H.; Li, Y. Diagnostic analysis and numerical simulation of a torrential rainstorm process caused southwestern low vortex. *Plateau Meteorol.* **2011**, *30*, 1158–1169.
5. Xiao, Y.H.; Yu, S.H.; Gao, W.L.; Xiao, D.X.; Xiao, H.R.; Shui, R. Cause analysis of one sustained into-the-sea Plateau Vortex accompanied by Southwest Vortex. *Plateau Meteorol.* **2018**, *37*, 1616–1627.
6. Li, Y.Q.; Xu, X.D.; Zhao, X.B. The theory and practice for observing design-layout of Southwest China vortex atmospheric scientific experiment. *Chin. Eng. Sci.* **2012**, *14*, 35–45.
7. Li, G.P.; Wan, J.; Lu, J.H. Potential mechanism of the warm vortex genesis in Southwest China. *J. Appl. Meteorol. Sci.* **1991**, *2*, 91–99.
8. He, G.B. Review of the Southwest Vortex Research. *Meteorol. Mon.* **2012**, *38*, 155–163.
9. Guo, M.Z. The statistic analyses on the easterly movement of plateau vortex. *Plateau Meteorol.* **1986**, *5*, 184–188.
10. Yu, S.H. New research advances of the Tibetan Plateau vortex in summer. *Torrential Rain Disasters* **2008**, *27*, 367–372.
11. Liu, X.Y.; Gong, Y.F.; Rren, Q.; Zhang, Q. Synergistic Effect of Tibetan Plateau Severe Convection and Tibetan Plateau Vortex Eastward-Propagating on the Downstream Heavy Precipitation Process. *Plateau Mt. Meteorol. Res.* **2024**, *44*, 10–20.
12. Li, S.S.; Li, G.P. Evolution and Mechanism Analysis of a Plateau Vortex and Plateau Shear Line. *Chin. J. Atmos. Sci.* **2017**, *41*, 713–726.
13. Zhang, Z.J.; Fan, G.Z. Relationship between Atmospheric Heat Source and the Plateau Vortex in the Eastern Tibetan Plateau. *J. Southwest Univ.* **2023**, *45*, 167–177.
14. Zheng, B.; Fan, G.Z.; Wu, Z.P.; Bai, H. Effect of Plateau Monsoon Strength on Plateau Vortex. *Mid-Low Latit. Mt. Meteorol.* **2021**, *45*, 15–22.
15. Chen, G.; Li, G.P.; Li, Y.Q. The Research Progress of the Tibetan Plateau Vortex in Recent Twenty Years. *Adv. Meteorol. Sci. Technol.* **2012**, *2*, 6–12.
16. Li, G.P.; Zhao, F.H. Analysis of 30-Year Climatology of the Tibetan Plateau Vortex in Summer with NCEP Reanalysis Data. *Chin. J. Atmos. Sci.* **2014**, *38*, 756–769.
17. Feng, X.Y.; Liu, C.H.; Rasmussen, R.; Fan, G.Z. A 10-yr Climatology of Tibetan Plateau Vortices with NCEP Climate Forecast System Reanalysis. *J. Appl. Meteorol. Climatol.* **2014**, *53*, 34–46. [CrossRef]
18. Lin, Z.Q.; Zhou, Z.B.; Jia, L. Objective Identifying Method of Qinghai-Xizang Plateau Vortex Using NCEP/NCAR Reanalysis Dataset. *Plateau Meteorol.* **2013**, *32*, 1580–1588.
19. Yu, S.H.; Gao, W.L. Analysis of Environmental Background and Potential Vorticity of Different Accompanied Moving Cases of Tibetan Plateau Vortex and Southwest China Vortex. *Chin. J. Atmos. Sci.* **2017**, *41*, 831–856.
20. Xiao, Y.Q.; Lou, P.X.; Li, M.J.; Wang, J.X. Analysis on a Heavy Rainstorm in Qinba Region Caused by Southwest Vortex and Northwest Vortex. *Plateau Meteorol.* **2023**, *42*, 98–107.
21. Kuo, Y.H.; Cheng, L.S.; Richard, A.A. Mesoscale Analyses of the Sichuan Flood catastrophe, 11–15 July 1981. *Mon. Weather. Rev.* **1984**, *114*, 1984–2003. [CrossRef]
22. Ma, X.D.; Zhi, X.F.; Wang, J.; Chen, J.; Feng, H.Z. Analysis of the Southwest Vortex activities in summer and their relationship with precipitation during the period of 1979–2016. *Trans. Atmos. Sci.* **2018**, *41*, 198–206.
23. Xiao, H.R.; Chen, J. Numerical study of one Plateau Vortex moving eastward affecting heavy rainfall in Sichuan. *Plateau Mt. Meteorol. Res.* **2010**, *300*, 12–17.
24. Wang, Z.; Wang, J.P. Climatic Characteristics of Southwest China Vortex and Its Impact on Rainstorm in Chongqing from 2012 to 2020. *Plateau Mt. Meteorol. Res.* **2024**, *44*, 128–133.
25. Liu, J.Q.; Liu, H.G.; Xu, J.Y. Analysis on Strong Convective Weather Triggered by Southwest Vortex. *Plateau Meteorol.* **2021**, *40*, 525–534.
26. Zhang, X.N.; Duan, X. Analysis on Southwest Vortex Rainstorm in Lower Latitude Plateau of China. *Plateau Meteorol.* **2005**, *24*, 941–947.
27. Zhou, C.H.; Xiao, D.X.; Yu, S.H. Circulation Background and Structural Characteristics of the Southwest Vortex Inducing Extreme Rainstorm in Sichuan Basin. *Meteorol. Mon.* **2022**, *48*, 1577–1589.
28. Cheng, L.S.; Guo, Y.H. Influence of Initial Conditions and Large-scale Topography on Mesoscale Simulation of the SW Vortex Evolution. *J. Lanzhou Univ. (Nat. Sci.)* **1990**, *26*, 140–147.
29. Pu, Y.K.; Guo, S.C.; Ma, L.X. The dynamical analysis of the generation and development of the southwest low vortex. *J. Yunnan Univ.* **1984**, *4*, 113–118.
30. Wang, B.; Isidoro, O. Study of a heavy rain vortex formed over the eastern flank of the Tibetan Plateau. *Mon. Weather. Rev.* **1987**, *115*, 1370–1393. [CrossRef]
31. Zheng, C.; Liu, Y.J.; Wang, Y.P.; Zhang, H.W.; Li, R.Q. Characteristics of rainstorm caused by southwest vortex in Qin-Ba Mountains in Shaanxi Province. *J. Shaanxi Meteorol.* **2024**, *1*, 24–28.

32. Zhang, Y.X.; Xu, D.B.; Li, Y.Q.; Li, Y.C.; Gao, L.; Yan, R.T. Research on the Characteristics of Typical 'Southwest Type' Basin Vortex in the Sichuan Basin. *Plateau Meteorol.* **2024**, *43*, 905–918.
33. Peng, X.D.; Cheng, L.S. A Case Numerical Study on the Evolution of the Low Vortex and Shear-line on the East Side of the PlateauII. Mesoscale Numerical Simulation. *J. Lanzhou Univ.* **1994**, *30*, 124–131.
34. Zhao, Y.C.; Wang, Y.H. A case study on plateau vortex inducing southwest vortex and producing extremely heavy rain. *Plateau Meteorol.* **2010**, *29*, 813–819.
35. Liu, Y.F.; Li, G.P. Climatic Characteristics of Atmospheric Heat Source over the Tibetan Plateau and Its Possible Relationship with the Generation of the Tibetan Plateau Vortex in the Summer. *Chin. J. Atmos. Sci.* **2016**, *40*, 864–876.
36. Fritsch, J.M.; Murphy, J.D.; Kain, J.S. Warm core vortex amplification over land. *J. Atmos. Sci.* **1994**, *51*, 1780–1987. [CrossRef]
37. Wang, B. Development mechanism for Tibetan Plateau warm vortices. *J. Atmos. Sci.* **1987**, *44*, 2978–2994. [CrossRef]
38. Chen, Z.M.; Miao, Q.; Min, W.B. A case analysis on mesoscale structure of severe southwest vortex. *J. Appl. Meteorol. Sci.* **1998**, *9*, 273–282.
39. Chen, G.; Li, G.P. The analyses of wave and eye region in Tibetan Plateau vortex. *Plateau Mt. Meteorol. Res.* **2010**, *30*, 6–11.
40. Yang, Y.C.; Li, Y.Q.; Chen, Y.R. The Characteristic Analysis of an Eastwards Plateau Vortex by Its Strengthening Process. *Plateau Meteorol.* **2018**, *37*, 702–720.
41. Huang, F.J. A composite analysis of the Southwest vortex. *Secentia Atmos. Sin.* **1986**, *10*, 402–408.
42. Fang, H.; Yuan, W.H.; Xu, Y.P. Three-Dimensional Circulation Structure in Advance of Summer Heavy Rainfall in the Middle-Lower Reaches of the Yangtze River. *Chin. J. Atmos. Sci.* **2020**, *44*, 761–775.

Disclaimer/Publisher's Note: The statements, opinions and data contained in all publications are solely those of the individual author(s) and contributor(s) and not of MDPI and/or the editor(s). MDPI and/or the editor(s) disclaim responsibility for any injury to people or property resulting from any ideas, methods, instructions or products referred to in the content.